NANO LETTERS

Letter

pubs.acs.org/NanoLett

Density of Trap States and Auger-mediated Electron Trapping in CdTe Quantum-Dot Solids

Simon C. Boehme,[†] Jon Mikel Azpiroz,[§] Yaroslav V. Aulin,[†] Ferdinand C. Grozema,[†] Daniël Vanmaekelbergh,[‡] Laurens D.A. Siebbeles,[†] Ivan Infante,[§] and Arjan J. Houtepen*[,†]

[†]TU Delft, Chemical Engineering, Optoelectronic Materials, Julianalaan 136, 2628 BL Delft, The Netherlands

[§]Kimika Fakultatea, Euskal Herriko Unibertsitatea (UPV/EHU) and Donostia International Physics Center (DIPC), P.K. 1072, 20018 Donostia, Euskadi, Spain

[‡]Utrecht University, Debye Institute, Condensed Matter and Interfaces, P.O. Box 80.000, 3508 TA Utrecht, The Netherlands

Supporting Information

ABSTRACT: Charge trapping is an ubiquitous process in colloidal quantum-dot solids and a major limitation to the efficiency of quantum dot based devices such as solar cells, LEDs, and thermoelectrics. Although empirical approaches led to a reduction of trapping and thereby efficiency enhancements, the exact chemical nature of the trapping mechanism remains largely unidentified. In this study, we determine the density of trap states in CdTe quantum-dot solids both experimentally, using a combination of electrochemical control of the Fermi level with ultrafast transient absorption and time-resolved photoluminescence spectroscopy, and theoretically, via density functional theory calculations. We find a high density of very efficient electron traps centered ~0.42 eV above the valence band. Electrochemical filling of these traps increases the electron lifetime and the photoluminescence quantum yield by more than an order of magnitude. The trapping rate constant for holes is an order of magnitude lower that for electrons. These observations can be explained by Auger-mediated electron trapping. From density functional theory calculations we infer that the traps are formed by dicoordinated Te atoms at the quantum dot surface. The combination of our unique experimental determination of the density of trap states with the theoretical modeling of the quantum dot surface allows us to identify the trapping mechanism and chemical reaction at play during charge trapping in these quantum dots.

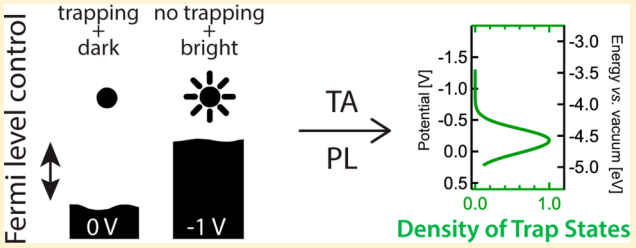

KEYWORDS: *quantum dot, defect, Auger-mediated trapping, electrochemistry, density functional theory, ultrafast spectroscopy*

Charge trapping is common in colloidal quantum-dot (QD) films and a major loss mechanism in optoelectronic devices in general as trapping often leads to recombination and the loss of charge carriers. In devices made of crystalline bulk materials the most common trapping sites are impurities or defects of the crystal structure such as vacancies or interstitial atoms. However, in multi- and nanocrystalline materials, surface defects play a dominant role. In CdTe solar cells, for example, grain boundaries were identified as the major defect site. Strategies to decrease the associated losses include grain growth[1] (i.e., diminishing the number of grain boundaries) and electronic passivation with $CdCl_2$ or $MgCl_2$.[2] In devices employing QDs, surface defects are even more important as the surface area is very high. Therefore, a large body of empirical work reported recipes for electronic passivation, using inorganic shells or ligand exchange.[3] Until now, only a few (largely theoretical) studies propose an explanation of the physical and chemical processes responsible for trapping.[4−7] The exact nature of the involved surface traps remains poorly understood. On the experimental side, measurements of the density of states (DOS) within the band gap are rare,[8−10] and on the theoretical side, the calculation of the surface for realistic QD sizes with realistic ligands remains a challenge.[5,11] A deeper understanding of charge trapping is necessary to advance the science and application of QDs.

In this study, we assess the density of trap states (DOTS) throughout the band gap in films of CdTe QDs using a novel combination of electrochemical control of the Fermi level and ultrafast transient absorption (TA) and time-resolved photoluminescence (PL) spectroscopy. Previous (often steady-state) spectroelectrochemical studies have already demonstrated PL brightening[12−15] and reduced blinking[16−20] under electrochemical filling of electron traps. Recently, our own group has shown that electron trapping in QD films can be slowed down by 3 orders of magnitude by electrochemically filling trap states.[21] Here, we extend these studies with ultrafast TA and PL experiments to determine the electron and hole trapping rates as a function of Fermi level. From a detailed energy-dependence of these rates we derive the density of available traps. This allows us to map the DOTS throughout the band

Received: January 6, 2015
Revised: March 27, 2015
Published: April 8, 2015

DOI: 10.1021/acs.nanolett.5b00050
Nano Lett. 2015, 15, 3056−3066

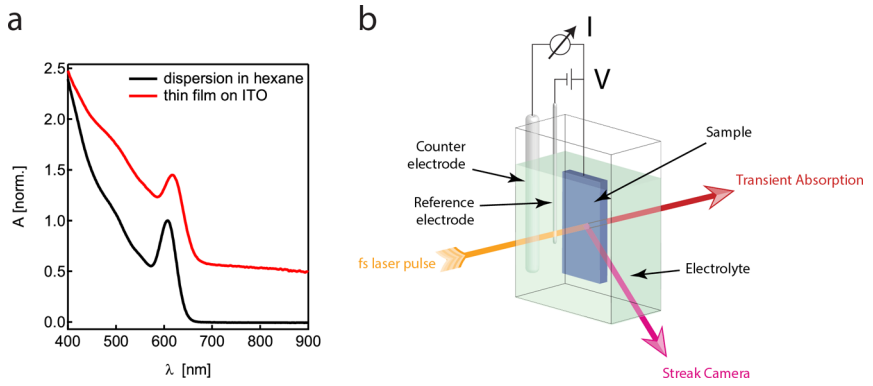

Figure 1. (a) Linear absorption spectrum, normalized at the $1S_{3/2}1S_e$ peak, for CdTe QDs with original ligands in hexane (black line) and as a film with 7DA ligands (red line). For clarity, spectra are offset vertically. (b) Schematic of the experiment: the Fermi level of the sample is controlled by the applied voltage in an electrochemical cell, whereas spectroscopic information is collected either by a streak camera or a transient absorption setup.

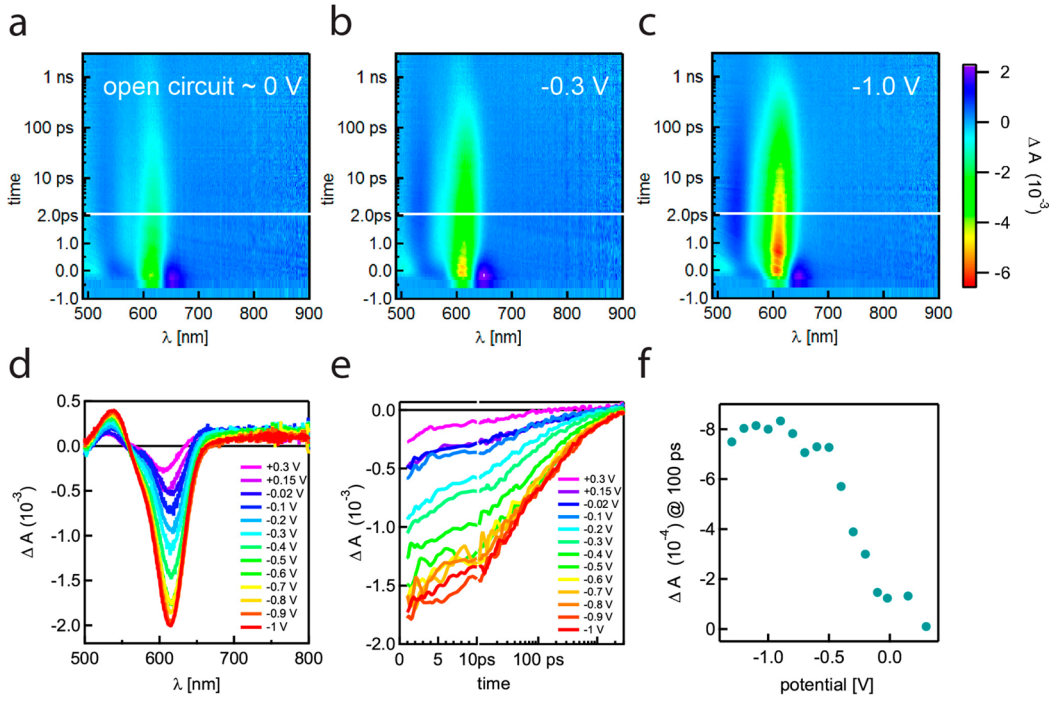

Figure 2. TA images after 400 nm excitation for a film of 7DA treated CdTe QDs with a diameter of 3.7 nm at (a) open circuit = −0.02 V, (b) −0.3 V, and (c) −1.0 V vs Ag wire, after excitation at 400 nm with a fluence of 2.0×10^{13} photons per cm^2 per pulse. (d) Spectra averaged from 10 ps to 3 ns, (e) kinetics at the $1S_{3/2}1S_e$ transition, and (f) $1S_{3/2}1S_e$ bleach at 100 ps, for all applied potentials. Both (e) and (f) show the transient absorption averaged between 590 and 700 nm.

gap. We find a DOTS that is well described by a Gaussian centered ∼0.42 eV above the valence band edge. Density functional theory (DFT) calculations relate the experimentally determined DOTS to the configuration of Te atoms at the surface, allowing for a complete picture of surface trapping. Surprisingly, the subgap states near the valence band act as very efficient electrons traps, whereas hole trapping is an order of magnitude slower. This discrepancy can be explained by Auger-mediated electron and hole trapping.

Results and Discussion. Figure 1a shows linear absorption spectra of CdTe QDs of 3.7 nm diameter dispersed in hexane with oleic acid (OA) ligands (black line) and deposited as a film, with ligands exchanged to 1,7-heptanediamine (7DA, red line). A film on an indium-doped tin oxide (ITO) substrate has been obtained using a layer-by-layer (LbL) dip-coating procedure as explained in the Experimental Section. Both spectra were normalized to one at the $1S_{3/2}1S_e$ peak and offset for clarity. In the film, quantum confinement is preserved as the $1S_{3/2}1S_e$ peak remains a pronounced feature of the absorption spectrum.

Figure 1b sketches the experimental procedure. The QD film on ITO substrate is immersed in an electrochemical cell (see Experimental Section). The Fermi level of the QD films is controlled by the applied voltage between the ITO working electrode and the pseudoreference electrode (−4.75 eV vs vacuum). The porous nature of the QD film causes electrolyte ions to permeate the whole film.[22,23] This allows for homogeneous charging and, hence, a constant shift of the Fermi level with respect to conduction and valence band, throughout the film. The electrochemical cell is placed in a fs

DOI: 10.1021/acs.nanolett.5b00050
Nano Lett. 2015, 15, 3056−3066

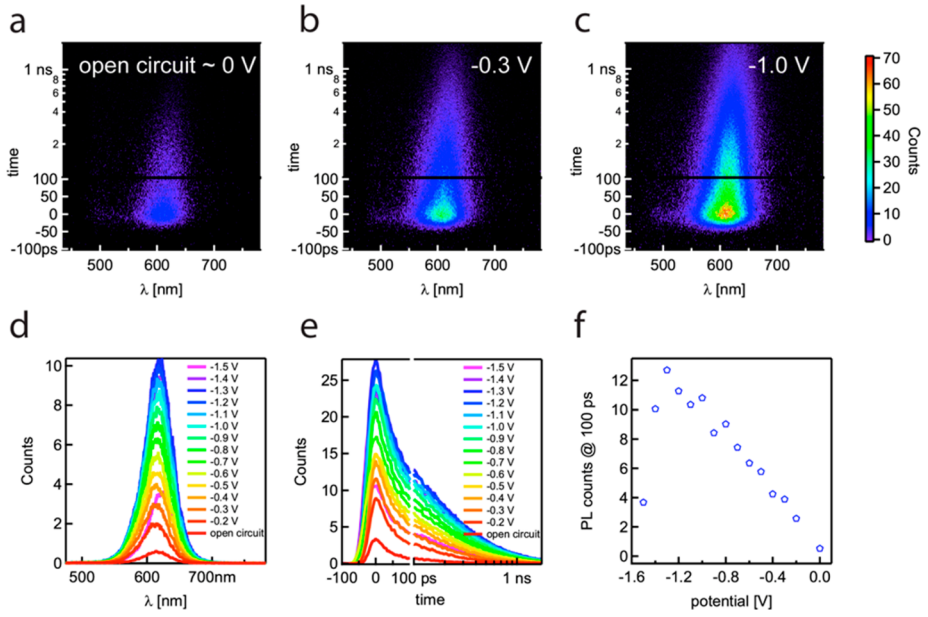

Figure 3. Streak camera PL images for a film of 7DA treated CdTe QDs with 3.7 nm diameter at (a) open circuit = −0.02 V, (b) −0.3 V, and (c) −1.0 V vs Ag wire pseudoreference electrode, after excitation at 400 nm with a fluence of 4.8×10^{13} photons per cm^2 per pulse, (d) spectra averaged over all time delays, (e) kinetics at the $1S_{3/2}1S_e$ transition, averaged from 550 to 700 nm, and (f) PL counts in (e) at 100 ps.

TA or a streak camera setup to perform ultrafast optical measurements. TA measurements are performed to determine the electron trapping rates and PL measurements to determine the hole trapping rates. This is motivated by the fact that for our CdTe QD films, TA is mainly sensitive to the $1S_e$ electron,[21,24−26] whereas PL is equally sensitive to $1S_e$ electron and $1S_{3/2}$ hole.

Figure 2a−c show 2D TA images for a film of 7DA capped CdTe QDs, which display the change in absorbance ΔA as a function of probe wavelength and time delay between the probe pulse and a 400 nm pump pulse with a fluence of 2.0×10^{13} photons per cm^2 per pulse. Figure 2a shows the response at open circuit potential (−0.02 V vs the Ag pseudoreference electrode), where the dominant feature is an absorption bleach ($\Delta A < 0$) of the $1S_{3/2}1S_e$ transition at 610 nm. This corresponds to an electron occupying the $1S_e$ state or a hole occupying the $1S_{3/2}$ state. For cadmium chalcogenide QDs, it has been shown that the $1S_{3/2}1S_e$ bleach is dominated by electrons.[21,24−26] It has been proposed that this is due to the fact that the DOS near the valence band edge is much higher than the DOS near the conduction band edge. As a result a single electron results in a much larger bleach than a single hole. It has been demonstrated that the hole contribution can be neglected and that the observed TA signal only originates from $1S_e$ electrons.[21,25,26]

Apart from the $1S_{3/2}1S_e$ bleach, a broad photoinduced absorption (PA) "shelf" feature[27−29] within the band gap is observed as well as red shifts of all optical transitions in the spectrum.[25−27] These features have all been observed and explained before. We focus on the $1S_{3/2}1S_e$ bleach feature, as its time evolution represents the decay of electrons from the $1S_e$ level. As shown in Figure 2a and e, this decay is on the order of tens of picoseconds and therefore much shorter than the radiative lifetime of 22.2 ns.[30] Hence, the decay must be nonradiative in nature. Following the argumentation in our previous work,[21] we assign it to electron trapping. This is in line with earlier reports, where electron trapping in ZnSe- and Mn^{2+}-doped ZnSe QDs has been reported to appear on a similar time scale.[12,13]

When the potential is decreased to −0.3 V, that is, the Fermi level is raised toward vacuum by 0.3 eV, the bleach becomes more pronounced and its lifetime longer, see Figure 2b. The trend continues when the potential is further decreased to −1.0 V (Figure 2c). A full dependence on the potential is given in Figure 2d and e, which displays the TA spectra (averaged between 10 ps and 3 ns) and the kinetics (averaged between 590 and 700 nm), respectively.

Figure 2e shows that, upon filling the electron traps (i.e., when the potential is decreased), both the electron lifetime and the maximum bleach increase. (See also Figure 4a for normalized TA transients, where the lifetime change is more clearly visible.) The former indicates slower trapping on a pico- to nanosecond time scale, the latter points toward less subpicosecond trapping, as such fast trapping is in competition with electron cooling to the $1S_e$ state and reduces the maximum transient occupation of the $1S_e$ level.

Figure 2f summarizes the effect by displaying the bleach 100 ps after excitation for all applied voltages. Note that the choice for 100 ps delay is arbitrary and similar results are obtained at other delay times. The bleach increases monotonously when the potential is decreased, down to −1.3 V. This is due to electrochemical filling of traps. When the traps are filled with electrons, electron trapping is reduced, resulting in longer electron lifetimes. The largest increase occurs between 0 and −0.5 V. Hence, in this potential range a large density of trap states must exist. Below −1.3 V, the signal reduces. Auger recombination between charges electrochemically injected in the $1S_e$ level and the photogenerated exciton could in principle explain the reduced bleach at negative potentials. For certain materials (e.g., for PbS QD films), we do indeed observe this. However, the electrochemical injection of electrons in the $1S_e$ level should result in a steady state bleach of the $1S_e1S_{3/2}$ transition and such a bleach does not occur here. Therefore, Auger recombination is discarded. Instead, we suggest that the decrease in the observed transient absorption bleach is due to

DOI: 10.1021/acs.nanolett.5b00050
Nano Lett. 2015, 15, 3056−3066

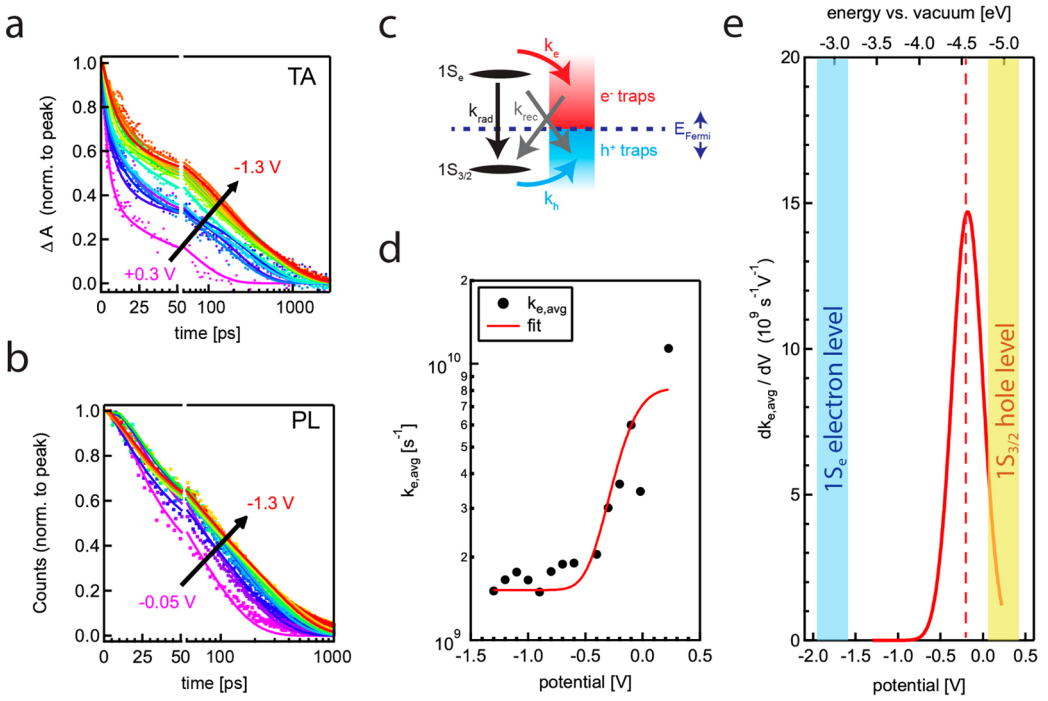

Figure 4. Normalized TA (a) and PL kinetics (b) at selected potentials. The time axis is linear up to 50 ps and logarithmic afterward. Data points are depicted by markers, whereas solid lines depict fits using the rate model sketched in (c) and explained in the main text. All trapping rate constants are allowed to depend on the Fermi level in the film which is given by the applied voltage. (d) Average electron trapping rate constant ($k_{e,avg}$, black solid circles), calculated according to refs 33 and 34 from the fit results for all electron trapping rate constants. The potential dependence is fitted globally with an error function and depicted by a red solid line (see Supporting Information). (e) Derivative of the fitted error function (red solid line) and the estimated position of the $1S_e$ level (blue shaded region) and $1S_{3/2}$ level (yellow shaded region), respectively.

the reduction of Cd^{2+} and a concomitant irreversible dissolution of the CdTe QD film.[31]

As we have argued previously,[21] the physical origin of the observed electron traps most likely lies in insufficient surface passivation. We believe that the dip-coating procedure used to grow these films leads to partial removal of ligands and incomplete recapping of the freed surface with new ligands (7DA in this case). Below, we will show strong evidence for this scenario.

To investigate the position of the DOTS with respect to valence and conduction band, we determined the energy of the $1S_{3/2}$ level spectro-electrochemically via a steady-state absorption bleach of the $1S_{3/2}1S_e$ transition upon shifting the Fermi level downward (see Figure S2 in the Supporting Information). The $1S_{3/2}$ level lies at +0.25 V, that is, at −5.0 eV vs vacuum. The energy of the $1S_e$ level (−1.75 V or −3.0 eV vs vacuum) is estimated by adding the optical band gap (~2.0 eV). A direct spectro-electrochemical determination of this level was not possible due to the low reduction potential of Cd^{2+} in CdTe, leading to irreversible dissolution of the film prior to electron injection into the $1S_e$ level.[31] Our own determination of the $1S_e$ and $1S_{3/2}$ levels is in line with previous assessments.[32] Therefore, we conclude that the large DOTS is located in the lower part of the band gap, close to the $1S_{3/2}$ level. We note that the Fermi level in dry CdTe QD films is close to the $1S_{3/2}$ level. This was determined by comparing the electron dynamics in TA experiments on dry films with those of electrochemically controlled films. At ~0 V the electron dynamics are identical implying that the Fermi level in the dry film is 0 V vs the Ag pseudoreference electrode, that is, 0.25 V above the $1S_{3/2}$ level. Thus, the dry film appears to be unintentionally p-doped, its Fermi level is below the DOTS and empty traps are available for electron trapping.

As the TA measurements do not reveal hole dynamics, we also performed time-resolved PL measurements with a streak camera setup. PL is equally sensitive to the presence of $1S_{3/2}$ holes as it is to $1S_e$ electrons because both are required for emitting a photon. Hence, both the hole and the electron decay are represented in the PL kinetics. Figure 3a−c displays time- and wavelength-resolved PL images at open circuit potential (−0.05 V), −0.3 V, and −1.0 V, respectively, after excitation at 400 nm with a fluence of 4.8×10^{13} photons per cm^2 per pulse.

The main feature in the PL images is emission at the $1S_{3/2}1S_e$ transition, whose intensity and lifetime increase when the Fermi level is moved toward vacuum. Figure 3d shows spectra at several potentials, averaged over all time delays. For all potentials, emission from the band gap, around 620 nm, is dominant, with an intensity that increases with decreasing potential. Below −1.3 V, as in the TA measurements, the signal decreases again, which might be explained by sample degradation.[31] Figure 3e reproduces the trend of the TA measurements: in the $1S_{3/2}1S_e$ kinetics, averaged from 550 to 700 nm, both the PL peak and lifetime increases with decreasing potential, down to −1.3 V (see also Figure 4b for normalized PL transients). Figure 3f displays the PL counts at 100 ps: at this time delay almost no PL is detected at open circuit potential (−0.05 V), whereas the PL signal is increased by a factor 85 at −1.3 V. Overall, the PL quantum yield increases by a factor 20, as inferred from integrating the PL image with respect to time and wavelength.

Formally the rate of electron trapping depends on the concentration of electrons n_e, the concentration of empty available traps $n_{trap,empty}$ and a rate constant c_e as follows:

DOI: 10.1021/acs.nanolett.5b00050
Nano Lett. 2015, 15, 3056−3066

$$\Gamma_{e,trap} = c_e \cdot n_e \cdot n_{trap,empty}(E_f) \approx k_e(E_f) n_e \quad (1)$$

For a given concentration of empty traps, and assuming that $n_e \ll n_{trap,empty}$ as will be the case at low excitation density, this is a quasi-first-order reaction. For this reason the concentration of traps is usually not written explicitly but included in a quasi-first-order rate constant k_e. Here, we use the term rate constant for both k_e and c_e unless it is specifically required to make the distinction.

The number of empty traps available for electron trapping is a function of the Fermi level. Therefore, we express the quasi-first-order rate constants for charge capture at a trap at energy E_t as $k_e(E_t,E_F) = c_e \cdot (1 - f(E_t - E_F)) \cdot N\rho$ for the electron and $k_h(E_t,E_F) = c_h \cdot f(E_t - E_F) \cdot N\rho$ for the hole, with c_e and c_h the electron and hole capture rate constants, respectively, $f(E_t - E_F)$ the trap occupation according to Fermi–Dirac statistics, N the number of traps per QD, and ρ the (normalized) density of trap states. Within this picture, electron ($\tau_e = 1/k_e$) and hole ($\tau_h = 1/k_h$) lifetimes both change with Fermi level, but inversely. The PL intensity is proportional to the product of electron and hole concentrations, $I_{PL} \propto n_e \cdot n_h \propto \exp(-(k_e + k_h) \cdot t) = \exp\{-[c_e + (c_h - c_e) \cdot f(E_t - E_F)] \cdot N\rho \cdot t\}$. If we assume for the moment that c_e and c_h are independent of energy, it is found that for equal capture rate constants ($c_e = c_h$), the PL lifetime is independent of Fermi level; for $c_e > c_h$, it increases with increasing Fermi level; and for $c_e < c_h$, it decreases with increasing Fermi level. The observed increase of PL intensity and lifetime with increasing Fermi level lets us conclude that the capture rate constant for electrons is much higher than for holes and that the PL quenching is dominated by electron trapping.

Fitting of Electron and Hole Dynamics. We now quantify the electron and hole trapping rates by fitting the TA and PL kinetics. Both data sets are simulated with the model sketched in Figure 4c. Herein, a $1S_e$ electron can decay either via radiative recombination with a $1S_{3/2}$ hole with rate constant k_{rad} or via trapping to an available electron trap with rate constant k_e. The ground state is recovered by recombination with a $1S_{3/2}$ hole with rate constant k_{rec}. Similarly, a $1S_{3/2}$ hole can decay via radiative recombination with a $1S_e$ electron with rate constant k_{rad} or via trapping to an available hole trap with rate constant k_h, from where it may recombine with a $1S_e$ electron with rate constant k_{rec}. The quasi-first-order rate constants k_e and k_h are a function of the Fermi level.

The observed kinetics are clearly not single exponential. We attribute this to sample inhomogeneity. Individual QDs will contain a variable number of unpassivated surface sites that lead to trapping and, consequently, will have varying trapping rates. We model this inhomogeneity by simulating the observed ensemble population by a sum of three subpopulations, indicated with indices i = 1, 2, and 3: one with fast trapping, one with intermediate trapping, and one with slow trapping. We do not imply that there are three separate trapping rates. These three rates are simply used to model the distribution of trapping rates in a mathematically simple way. Modeling a continuous distribution of trapping rates by a sum of exponentials has previously been performed and justified by Jones et al.[33,34]

We fit TA and PL data after 2 ps, when charges have relaxed to the respective band edges. Then, the charge occupation in the QD films can be described by the densities of three species: QDs with a $1S_e$ electron and a $1S_{3/2}$ hole ($n_{eh,i}$), QDs with a $1S_e$ electron and a trapped hole ($n_{e0,i}$), and QDs with a trapped electron and a $1S_{3/2}$ hole ($n_{0h,i}$), where the index i denotes the subpopulations of QDs with fast, intermediate and slow trapping, respectively. The time evolution of the densities is obtained from the model sketched in Figure 4c, yielding the following rate equations

$$\frac{dn_{eh,i}}{dt} = -(k_{rad} + k_{e,i} + k_{h,i}) \cdot n_{eh,i} \quad (2)$$

$$\frac{dn_{e0,i}}{dt} = +k_{h,i} \cdot n_{eh,i} - (k_{e,i} + k_{rec}) \cdot n_{e0,i} \quad (3)$$

$$\frac{dn_{0h,i}}{dt} = +k_{e,i} \cdot n_{eh,i} - (k_{h,i} + k_{rec}) \cdot n_{0h,i} \quad (4)$$

As discussed above, the TA kinetics of the $1S_{3/2}1S_e$ bleach represent the $1S_e$ electron decay, whereas the PL kinetics represent both $1S_e$ electron decay and $1S_{3/2}$ hole decay. Hence, the TA signal is given by

$$\Delta A(t) \propto \sum_{i=1}^{3} (n_{eh,i}(t) + n_{e0,i}(t)) \quad (5)$$

and the PL signal by

$$I_{PL}(t) = \sum_{i=1}^{3} n_{eh,i}(t) \quad (6)$$

The TA decay contains fewer parameters as it does not distinguish between $n_{eh,i}$ and $n_{e0,i}$ and is effectively independent of hole trapping. Hence, we start by modeling the TA data. Figure 4a shows TA data (closed circles), normalized to the peak signal, and fits (solid lines) from +0.3 V to −1.3 V. The fit results for the high ($k_{e,1}(E_F)$), intermediate ($k_{e,2}(E_F)$) and small ($k_{e,3}(E_F)$) electron-trapping rate constants are shown in Supporting Information Figure S3. As shown in that figure the rate constants $k_{e,i}$ vary by 2 orders of magnitude, but their potential dependence is identical within the noise of the measurement. This suggest that the nature of the trapping process is the same in all cases, or at least that the trap energy is very similar, and supports our initial assumption that the three trapping rates represent QDs with a different number of the same traps. The broad distribution of trapping times implies that there is a broad distribution of available traps. There is likely a significant variation of the number of traps per QD. In addition, charges in these conductive QD solids are mobile[35] and may diffuse around before encountering a trap. A variation in local electron mobilities due to disorder in the film will further broaden the distribution of observed trapping rates.

As the three rate constants likely represent trapping at similar traps, we represent them by a single average electron trapping rate constant, obtained according to Jones et al.[33,34] (see Supporting Information for details). This average electron trapping rate constant is shown as black solid circles in Figure 4d. As expected, electron trapping monotonously decreases when the Fermi level is moved toward vacuum, to more negative potentials.

PL decay is determined by the same electron trapping processes that causes the decay of TA, while additionally hole trapping accelerates PL decay. We therefore fix the electron trapping rate constants, the recombination rate constant and the population fractions $n_{eh,i}/(\sum_{i=1}^{3} n_{eh,i})$, $n_{e0,i}/(\sum_{i=1}^{3} n_{e0,i})$, and $n_{0h,i}/(\sum_{i=1}^{3} n_{0h,i})$ to the respective values obtained from the TA fit, leaving the hole trapping rates $k_{h,i}(E_F)$ as the only free parameters. The fits to the normalized PL decays from −0.05 V

DOI: 10.1021/acs.nanolett.5b00050
Nano Lett. 2015, 15, 3056−3066

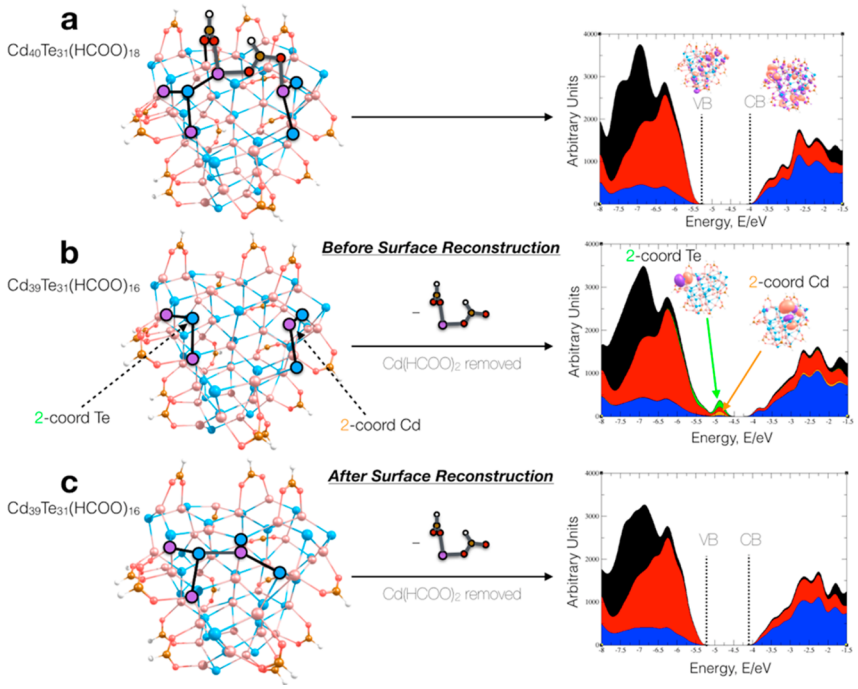

Figure 5. (a) Fully passivated $Cd_{40}Te_{31}(HCOO)_{18}$ QD and its DOS (pink = Cd, blue = Te, red = O, brown = C, and white = H atoms), (b) CdTe QD and its DOS after removal of one $Cd(HCOO)_2$ and *before* surface reconstruction, and (c) CdTe QD and its DOS after removal of one $Cd(HCOO)_2$ and *after* surface reconstruction. All calculations have been performed with DFT at the PBE/def2-SV(P) level of theory. The colors in the DOS panels indicate contribution from the ligands (black), the Te atoms (red) and the Cd atoms (blue). In panel (b) the contribution of the dangling 2-coordinated Te (green) and Cd (orange) atoms has also been included.

to −1.3 V are shown in Figure 4b. Hole trapping rate constants are on the order of 10^{10} s^{-1}, 10^{9} s^{-1}, and 10^{8} s^{-1} for the three subpopulations of QDs (see Supporting Information Figure S3) and are, in each case, an order of magnitude lower than the electron trapping rate constants.

Most hole trapping occurs beyond the 1 ns time scale of the experiment. Further, both the TA and the PL decay are dominated by electron trapping. This makes the fits less sensitive to hole trapping than to electron trapping and precludes a quantitative assessment of the Fermi level dependence of the hole trapping rate constant.

To most accurately determine the density of trap states, we globally fitted an error function to the electron trapping rate constants using the reciprocal standard deviation of the fitted rate constant as weight factor (see Supporting Information Figure S3). The resulting error function is shown as a red solid line in Figure 4d. The rationale behind using an error function is that its derivative, a Gaussian function, would likely describe the DOTS accurately. This Gaussian is shown in Figure 4e. Its center is located at −0.18 V (−4.57 eV vs vacuum or 0.43 eV above the $1S_{3/2}$ level) and its fwhm is 0.42 V. The position of the $1S_e$ electron and $1S_{3/2}$ hole level is marked with a blue and yellow shaded region, respectively. The width of the shaded regions indicates the estimated uncertainty in the exact position of those levels.

DFT Calculations Relate Trapping to Structural Properties of the QD Surface. We now relate the observed DOTS to structural properties of the nanocrystal surface via DFT calculations. The prevailing picture in the literature is that sufficient ligand coverage is key for electronically passivating the otherwise defect-rich QD surface.[27,36−40] This is in line with PL quantum yield measurements for CdSe QDs from the group of Weiss[39] and with time-resolved PL and TA data of CdTe QDs from our own group.[21] These studies show that an increasing number of purification steps in the postsynthesis treatment decreases the PL quantum yield and accelerates charge trapping, attributed to a loss of ligands. Owen's group has shown that the dependence of PL quantum yield on ligand coverage is superlinear, suggesting that a few missing ligands can be compensated by surface reconstruction, whereas ligand removal above a certain threshold leads to surface states within the band gap.[36] We consider that the same applies to the CdTe QD films studied here. Film formation includes extensive exposure to methanol and replacing ligands (1,7-heptanediamine). Both could induce the removal of ligands from the CdTe surface, probably in the form of Z-type Cd-$(oleate)_2$.[36,37]

The reference QD model for our DFT calculations has been constructed by cleaving a zincblende CdTe lattice from which we have extracted a nonstoichiometric QD cluster, $Cd_{40}Te_{31}$, of about 1.5 nm in size. This model displays a Cd:Te ratio of 1.29, a ligand coverage of about 2.9 nm^{-2} and a pseudopyramidal shape (see Figure 5a). Charge neutrality in the model system is maintained by adding 18 formate anions, $HCOO^-$, to emulate the native oleate ligands and to compensate for the excess Cd^{2+} ions. This model shows a significant geometrical reconstruction on the surface after addition of the formate anions, however preserving the underlying zincblende shape.

The DOS of this system is also shown in Figure 5: the HOMO and LUMO are delocalized orbitals and no states appear in the band gap. We note that Cd and Te are 4-coordinated in the center of the cluster and 3-coordinated at the surface. This lower coordination apparently does not lead to dangling bonds inside the band gap; the corresponding orbitals have energies inside the conduction and valence bands.

From the fully relaxed structure of $Cd_{40}Te_{31}(HCOO)_{18}$, we subsequently remove one Cd atom and two formate anions to

DOI: 10.1021/acs.nanolett.5b00050
Nano Lett. 2015, 15, 3056−3066

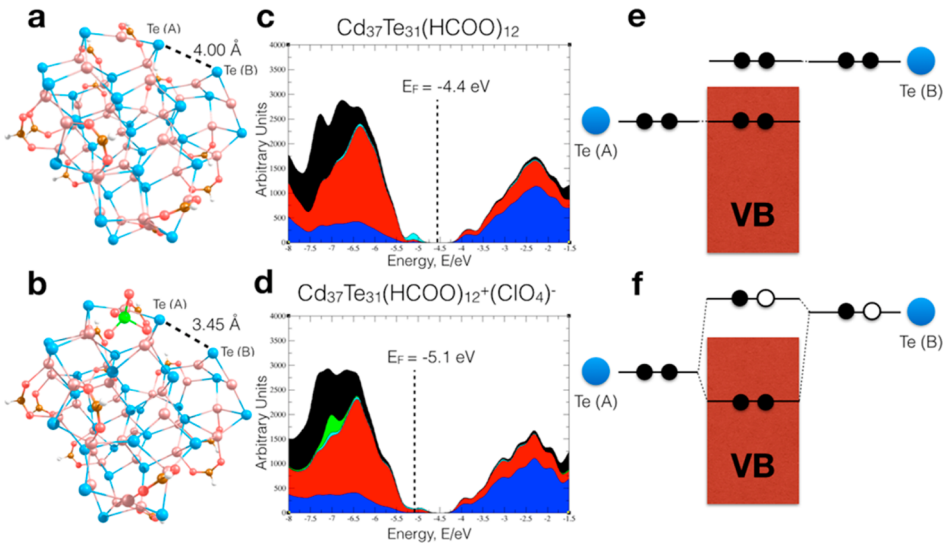

Figure 6. (a)−(b) Fully relaxed structures for the neutral and oxidized CdTe QD models, respectively, and (c)−(d) their DOS. (e)−(f) Schematic molecular orbital diagrams that show the interaction between a 3-coordinated Te atom, Te (A), and the adjacent undercoordinated Te atom, Te(B), for the neutral and oxidized species. In the latter case a weakly bonded dimer is formed. The antibonding orbital is only partially occupied and can also act as an electron trap.

simulate Z-type ligand removal. Afterward, the system is allowed to reconstruct and find its most stable structure. The DOS before and after surface reconstruction is shown in Figure 5. The eye-catching feature is that, before surface reconstruction (Figure 5b), the QD features two 2-coordinated dangling Te and Cd atoms, which are described by two molecular orbitals (one occupied and the other empty) close to the valence band edge and mostly localized on the 4p and 5s orbitals of the Te and Cd atoms, respectively. This shows that 2-coordinated surface atoms do form states in the band gap. Because the two 2-coordinated surface atoms are spatially close to each other, after reconstruction, the occupied 4p orbital on Te donates its electrons to the empty 5s orbital on Cd and forms a bond (see Figure 5c). In this case, both Te and Cd increase their coordination number and their orbitals delocalize inside the conduction and valence band, removing the midgap states. The QD has self-healed.

As shown in the Supporting Information, self-healing via surface reconstruction is no longer possible once several ligands have been removed. After removal of three $Cd(HCOO)_2$, the number of trap states increases linearly with the number of removed $Cd(HCOO)_2$. The computed structure reveals undercoordinated Te atoms as the origin of the traps, whereas Cd atoms always remain sufficiently coordinated. As a result a large DOTS is formed near the valence band, consisting of 2-coordinated Te surface orbitals. The position of this DOTS is in agreement with the experimentally observed DOTS, suggesting that insufficient ligand coverage and 2-coordinated Te atoms are responsible for charge trapping.

In our calculations, the computed DOTS lies below the Fermi level and can therefore only act as a source of hole traps. In the experiments, however, we find that many of the surface states are empty and act as electron traps (i.e., the QD films are unintentionally p-type). To simulate this, we computed the electronic structure of an oxidized $Cd_{37}Te_{31}(HCOO)_{12}^{+}$ model, featuring one dicoordinated Te atom. To avoid spurious effects from the excess of cationic charge, we add a perchlorate anion as a spectator ligand, which keeps the overall system neutral. The geometry and the computed DOS for this system are shown in Figure 6.

A first observation is that the oxidized QD (Figure 6b) presents a geometry similar to the neutral QD, with only one significant difference: the 2-coordinated Te atom, denoted as Te(B), is spatially closer to the 3-coordinated Te atom, Te(A). Oxidation shrinks the Te(A)−Te(B) bond length from 4.00 to 3.45 Å. To understand this, we plot a scheme of the molecular orbitals patterns for the neutral (Figure 6e) and oxidized (Figure 6f) species. When the QD cluster is neutral (i.e., the Fermi level is near midgap), the 5p orbital on Te is doubly occupied and remains mostly unbound. The loss of one electron implies the oxidation of the 5p orbital on Te(B), which becomes a weak electron acceptor. This orbital interacts with the closest electron donor in the neighborhood, that is, the 5p on Te(A), in a bonding/antibonding fashion. Note that the antibonding orbital is singly occupied, which means that (1) the Te−Te bond is weak, (2) this orbital can act as both electron and hole trap, and (3) the Fermi level is shifted toward the valence band.

One can generalize this view for larger QD, for which the number of undercoordinated Te atoms is high. A half-filled DOTS (as roughly the case in dry QD films in the experiments) means that many of these Te atoms are oxidized and form weakly bound Te−Te dimers on the QD surface each displaying a half-populated antibonding orbital that act both as electron and hole trap. Electrochemical filling of these traps breaks the Te−Te bonds, resulting in undercoordinated Te atoms at the QD surface, with 5p lone-pairs acting mostly as hole traps.

Auger-Mediated Electron Trapping. We now discuss in more detail how the electron and hole trapping rate constants depend on the DOTS and the energy loss involved in the trapping process. We start by expressing the electron trapping rate constant as

$$k_{e,avg}(E_F) = N \cdot \int_{-\infty}^{+\infty} \rho(E) \cdot (1 - f(E - E_F)) \cdot c_e(E) dE \quad (7)$$

DOI: 10.1021/acs.nanolett.5b00050
Nano Lett. 2015, 15, 3056−3066

As before, N denotes the respective number of traps per QD, $\rho(E)$ is the (normalized) DOTS, $f(E - E_F)$ the Fermi–Dirac distribution and $c_e(E)$ the capture rate constant of an electron by a trap at energy E. If we neglect thermal broadening of the Fermi–Dirac distribution at room temperature, because k_BT is smaller than our experimental potential step size (100 meV), eq 7 simplifies to

$$k_{e,avg}(E_F) = N \cdot \int_{E_F}^{E_{1Se}} \rho(E) \cdot c_e(E) dE \quad (8)$$

We restrict the upper integration bound to the $1S_e$ electron level, assuming that trapping only takes place at states within the band gap. For the hole, an equivalent reasoning holds, leading to $k_{h,avg}(E_F) = N \cdot \int_{E_{1S3/2}}^{E_F} \rho(E) \cdot c_h(E) dE$, where $c_h(E)$ is a hole specific capture rate constant. Therefore, the DOTS $\rho(E)$ can be retrieved from either electron or hole quasi-first-order trapping rates constants, via

$$\rho(E_F) = -\frac{1}{N c_e(E_F)} \cdot \frac{dk_{e,avg}(E_F)}{dE_F} \quad (9)$$

or equivalently *via* $\rho(E_F) = (N c_h(E_F))^{-1} \cdot (dk_{h,avg}(E_F))/dE_F$, as shown in the Supporting Information. As the electron trapping rates could be determined with greater accuracy, we chose the derivation from electron trapping rates. In eq 9, the index indicating the Fermi level may be omitted, because we neglect thermal broadening, that is, $\rho(E_F) = \rho(E)$.

A challenge lies in estimating the capture rate constant $c_e(E)$, for which the nature of the trapping process must be known. This is the topic of a lively discussion currently held in the literature. In the debate, several mechanisms have been proposed, ranging from resonant trapping[4,41] to shallow trapping[42] to deep trapping,[8,21,41,43] to either a single[42] or multiple defect states,[44] either described by Marcus theory, Marcus–Jortner theory,[42,45,46] or by Auger induced trapping.[4,41] To reveal which mechanisms is applicable to trapping in the QD films investigated here, we compare three scenarios: (1) the electron capture rate constant is constant in energy, (2) electron capture can be explained as an electron transfer process according to Marcus theory, and (3) electron capture is Scenario (3), i.e. Auger-mediated trapping, is shown schematically in Figure 7a.

Scenario (1) implies that our measurement presents a direct determination of the DOTS, as it would be equal to the (scaled) $dk_e(E_F)/dE_F$ shown in Figure 4e. Scenario (2) has previously been invoked by Mooney et al. to explain surface trapping in CdS, CdSe, and CdSe/ZnS QDs.[42,46] In these studies, the authors proposed a semiclassical Marcus–Jortner formalism with strong coupling of the surface state to the LO phonon (Huang–Rhys parameter ~10), a reorganization energy of 15 meV and a trap depth of 50 meV. Although the experimental approach could not distinguish between electron and hole trapping, their model successfully described the strong temperature dependence of the observed defect PL. In our case, however, this model fails, as the depth of the electron trap is much larger than the reorganization energy, on the order of 1.6 eV. As a result, both the Marcus and the Marcus–Jortner model predict unphysically low electron trapping rates and are unable to reproduce the picosecond electron lifetimes observed in TA and PL. For hole trapping, the situation is different: the trap depth is much smaller (~0.4 eV) and the hole-trapping rate is lower. In this case, trapping may possibly be explained by the Marcus or Marcus–Jortner model.

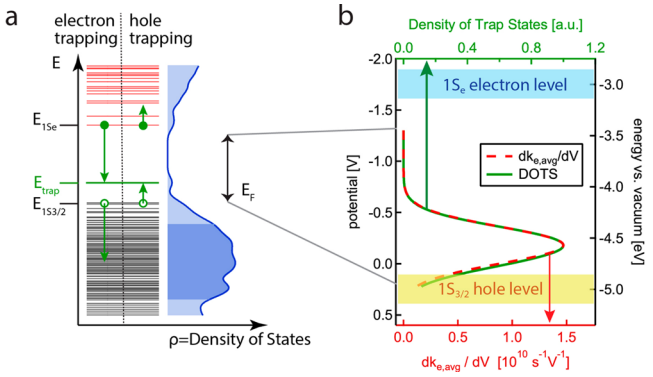

Figure 7. (a) Schematic of Auger-mediated electron and hole trapping to a trap state at the QD surface, at an energy close to the valence band edge. Assuming the matrix elements for electron and hole Auger-mediated trapping do not differ too much, electron trapping proceeds faster due to a larger density of acceptor states for the scattered hole (deep in the valence band) compared to a sparser density of acceptor states for the scattered electron (close to the conduction band edge). The occupied and unoccupied molecular orbitals (gray and red horizontal bars, respectively) and the density of states (light blue shaded area) were obtained from DFT calculations for a $Cd_{37}Te_{31}(HCOO)_{12}$ QD with insufficient ligand coverage (see main text). The dark blue shaded area depicts the hole acceptor states for the range of Fermi levels within our experimental probe window (double-headed arrow). (b) Derivative of the average electron trapping rate constant (red dashed line) and DOTS (green solid line) according to eq 9 and eq 10

Auger-mediated trapping is shown schematically in Figure 7a. This process involves the trapping of the electron (hole) by scattering with the geminate hole (electron). The energy difference in the trapping process is not dissipated to phonons but is given to the second charge carrier, which subsequently cools down to the band edge. Unlike the Marcus model, the Auger process permits large energy losses for the electron in the trapping process. From the schematic in Figure 7a , it is clear that one of the factors that determines the rate of this Auger trapping process is the DOS at the energy of the final hot charge carrier. Because hole trapping involves energy dissipation of ~0.4 eV this corresponds to the electron being promoted to a state ~0.4 eV above the $1S_e$ level, where the DOS will be low. For electron trapping the hole is excited to a state ~1.6 eV below the $1S_{3/2}$ level, where the DOS will be much higher. In addition the DOS in the valence band is much higher than the DOS in the conduction band. If the matrix elements for electron and hole Auger-mediated trapping do not differ too much, the result will be that the Auger trapping rate is much higher for electrons than for holes. Thus, we propose that Auger-mediated trapping can explain the observed order of magnitude difference in electron and hole trapping rates.

We quantify the rate of Auger-mediated electron trapping using Fermi's golden rule. For a process where the electron goes from its initial state at energy E_{1Se} to final state at energy $E = E_{1Se} - \Delta E$, by promoting a $1S_{3/2}$ hole to states deeper into the valence band, we obtain the following capture rate constant (see Supporting Information):

$$c_{e,Auger}(E) = \frac{2\pi}{\hbar} \cdot |M|^2 \cdot \rho(E_{1S_{3/2}} - \Delta E) \quad (10)$$

where $\rho(E_{1S_{3/2}} - \Delta E)$ is the density of valence band states at energy ΔE below the $1S_{3/2}$ level and M is the matrix element for this process (see Supporting Information).

DOI: 10.1021/acs.nanolett.5b00050
Nano Lett. 2015, 15, 3056–3066

The two factors determining the capture rate constant are, thus, the matrix element and the density of valence band states at energy ΔE below the $1S_{3/2}$ level. Inserting eq 10 into eq 8 yields the quasi-first-order electron-trapping rate constant k_e, which also depends on the density of trap states.

Califano at al. have shown that matrix elements for Auger-mediated trapping do not vary much with energy.[4] These authors considered hole trapping at relatively shallow trapping sites and the corresponding Auger excitation of electrons to $1P_e$ states. We propose that a similar process occurs for very deep traps. In that case, the higher DOS at the final energy of the scattered charge carrier would make this process even faster.

If we assume, following Califano et al., that the matrix element in eq 10 is constant then the energy dependence of the capture rate constant only comes from $\rho(E_{1S_{3/2}} - \Delta E)$. Auger-mediated electron trapping implies that about ~1.6 eV of energy is transferred to the hole. At these energies, the DOS in the valence band approaches the bulk DOS and will be independent of nanocrystal size. This allows us to use the DOS from the DFT calculation described above (for the cluster model $Cd_{37}Te_{31}(HCOO)_{12}$) to assess the energy dependence of Auger recombination. This DOS is shown in Figure 7a together with a schematic of the Auger process. It is clear that at the relevant energies in the valence band the DOS is high and relatively constant. Finally this allows us, by combining eq 10 with eq 9 to derive the DOTS from the measured electron trapping rate constants depicted in Figure 4e.

Figure 7b shows the normalized DOTS (green solid line) so obtained from the derivative of the fitted electron trapping rate (red dashed line, $dk_{e,avg}/dV$). The former closely resembles the shape of the latter. This is due to the rather flat DOS in the valence band at the final energies of the hole that is excited in the Auger-mediated trapping process (dark blue shaded region in Figure 7a). A Gaussian fit to the DOTS is centered at −4.58 eV vs vacuum (0.42 eV above the $1S_{3/2}$ level) and has a fwhm of 0.44 eV.

We conclude that a Marcus(−Jortner)-type trapping mechanism fails and an Auger-mediated trapping mechanism succeeds in explaining the observed fast electron trapping to deep traps, close to the $1S_{3/2}$ level. On first sight, this is in contrast to the Marcus−Jortner model with shallow traps proposed by Mooney et al.[42,46] However, these authors focused on CdSe QDs, where the details of surface trapping could be different from the CdTe QDs investigated here. In addition, differences could arise due to different Fermi levels. In the case presented here, the Fermi level was near the valence band, below the DOTS, leading to *electron* trapping via an Auger mechanism. In systems where the Fermi level is well above the density of trap states *hole* trapping may dominate, possibly via a Marcus−Jortner-type mechanism.

Conclusions. We report the first experimental determination of the density of trap states (DOTS) of a film of CdTe QDs, using a novel combination of electrochemistry and ultrafast spectroscopy. The occupation of traps within the band gap is controlled via reversible electrochemical doping and is monitored via transient absorption and time-resolved photoluminescence spectroscopy. When traps are empty, electron trapping proceeds on a (sub-)picosecond time scale; when traps are filled electrochemically, this process takes nanoseconds. We obtain the DOTS by fitting the decay of transient absorption and time-resolved photoluminescence signals at various Fermi levels within the band gap. A DOTS close to the valence band is found, 0.42 eV above the $1S_{3/2}$ level and with a fwhm of 0.44 eV. DFT calculations confirm a large DOTS close to the valence band and assign it to dicoordinated Te atoms at the QD surface as a result of a loss of ligands during film processing.

Time-resolved photoluminescence experiments reveal that hole trapping also occurs, albeit at least 1 order of magnitude slower than electron trapping. The slower hole trapping and the fast capture of electrons by traps close to the valence band can be explained by an Auger-mediated trapping mechanism.

The combination of our unique experimental determination of the DOTS with the theoretical modeling of the QD surface reveals the nature of the charge trapping mechanism in QD films. The assignment of the DOTS to the exact composition and geometry of the surface pinpoints the bottlenecks for improving QD based devices.

Experimental Section. *Materials.* 1,7-Heptanediamine (98%, Aldrich), methanol (anhydrous, 99.8%, Sigma-Aldrich), butanol (anhydrous, 99.8%, Sigma-Aldrich), acetonitrile (anhydrous, 99.8%, Sigma-Aldrich), $LiClO_4$ (battery grade, dry, 99.99%, Aldrich), Te (−18 + 60 mesh, 99.999%, Alfa Aesar), trioctylphosphine (97%, Aldrich), 1-octadecene (technical grade, 90%, Aldrich), and oleic acid (technical grade, 90%, Aldrich) were all used as received.

QD Synthesis. CdTe QDs with a diameter of 3.7 nm were synthesized following the procedure described by Kloper et al.[47] At 310 °C in N_2 atmosphere, a TOP (trioctylphosphine)−Te precursor in ODE (octadecene) is injected rapidly to a Cd-(oleate)$_2$ precursor in ODE under vigorous stirring. Growth took place at 270 °C and was stopped after several minutes by injection of cold toluene. The dispersion was purified by adding anhydrous MeOH and anhydrous BuOH as nonsolvents at a volume ratio of 1:1:2 (reaction solution:MeOH:BuOH) to precipitate the QDs in a centrifuge at 3500 rpm during 7 min. Subsequently, the precipitate was redispersed in chloroform and the whole purification procedure was repeated once.

Film Processing and Ligand Exchange. Films with 7DA ligands are grown on ITO substrates in a layer-by-layer (LbL) dip coating procedure using a mechanical dipcoater (DC Multi-8, Nima Technology) in a N_2 purged glovebox: the substrates were first immersed for 30 s in a concentrated (~10^{-5} M) QD dispersion, subsequently immersed for 30 s in a magnetically stirred 0.1 M solution of the 7DA ligand in MeOH, and finally dipped twice for 10 s in stirred MeOH to rinse excess ligands. Using this procedure, the original insulating ligands are replaced by the shorter bidentate ligands. The above procedure was repeated 10−20 times to yield films roughly 10−20 QD monolayers thick. A small region on the edge of the ITO substrate remained uncoated to provide electrical contact in electrochemical measurements.

Linear Absorption Spectra. Linear absorption spectra were recorded in a PerkinElmer λ 900 absorption spectrometer equipped with an integrating sphere to correct for scattering and reflection. Figure 1a shows linear absorption spectra of CdTe QDs of 3.7 nm diameter, either as a dispersion in hexane with oleic acid (OA) ligands (black line) or deposited as a film, with ligands exchanged to 1,7-heptanediamine (7DA, red line). Both spectra were normalized to one at the $1S_{3/2}1S_e$ peak and offset for clarity. In the film, quantum confinement is preserved, as the $1S_{3/2}1S_e$ peak remains a pronounced feature of the absorption spectrum.

Broadband Transient Absorption Measurements. Broadband transient absorption (TA) measurements were performed

DOI: 10.1021/acs.nanolett.5b00050
Nano Lett. 2015, 15, 3056−3066

in the low fluence limit (<0.1 excitations per QD, where the TA kinetics were independent of pump fluence) on a film with an optical density of about 0.25 at the pump wavelength to provide uniform excitation densities. The sample was excited in the electrochemical cell with ~180 fs pump pulses from an OPA (Light Conversion ORPHEUS) pumped by an amplified femtosecond laser (Light Conversion PHAROS SP), at a repetition rate of 2500 Hz. Absorption spectra in the visible (450−900 nm) were recorded with an Ultrafast Systems HELIOS spectrometer at a repetition rate of 5000 Hz using broadband probe pulses from a sapphire crystal pumped by the 1030 nm fundamental of the laser. A variable delay of −10 to 3000 ps between probe and pump pulses was introduced to yield difference absorption spectra, as a function of pump−probe delay and probe energy. Due to dispersion in optical components between the white light generating crystal and the photodetector, the "time zero", that is, the point of time where pump and probe show maximum temporal overlap, depends on the probe wavelength. Dispersion corrected 2D TA data with identical time zero for all wavelengths were obtained by subtracting a third-order polynomial fit to the "coherent artifact",[48,49] obtained on a blank ITO electrode in the same electrochemical cell, from the raw data. About 10 000 difference absorption spectra were obtained per pump−probe delay.

Streak Camera Measurements. Time- and wavelength-resolved photoluminescence (PL) measurements were performed using a streak camera (Hamamatsu C5680). The sample was excited with ~150 fs laser pulses from a Ti:sapphire laser (Chameleon Ultra by Coherent, Inc.), centered at 400 nm, at a repetition rate of 4 MHz. The pump beam was focused and had a diameter of about 40 μm at the position of the sample, leading to an excitation fluence of about 4×10^{13} photons per cm^2 per pulse. PL of the sample was collected in reflection geometry with a parabolic mirror, dumping the direct (specular) reflection via a hole in the center of the mirror. The collected PL was focused by a lens with 200 mm focal length and fed into a spectrograph (Princeton Instruments Acton SP2300) through an entrance slit with a width of 100 μm. The PL was then measured by the streak camera in the slow sweep mode, over a time window of about 2 ns.

Electrochemical Control of the Fermi Level. The Fermi level of our QD films on ITO was controlled by a CHI832B bipotentiostat (CH Instruments, Inc.) while immersed in an airtight quartz electrochemical cell with an Ag wire pseudoreference electrode and a Pt sheet counter electrode (see inset in Figure 1). The Ag wire pseudoreference electrode (−4.75 V vs vacuum) was calibrated against the ferrocene/ferrocinium couple.[50] In a N_2 purged glovebox, the cell is loaded with a QD film, filled with 0.1 M $LiClO_4$ in anhydrous acetonitrile and sealed with an O-ring to ensure air-free conditions. All chemicals were used as received. The electrochemical cell is placed such that TA measurements are possible, with both pump and probe beams passing through the front window, the QD films and the back window of the cell. Figure 1b sketches the experimental procedure. The Fermi level of the QD films is controlled by the applied voltage between the film and the pseudoreference electrode.

The porous nature of the QD films causes electrolyte ions to permeate the whole film.[22,23] In contrast to electrochemical experiments on 2D samples, 3D porous QD films are fully depleted allowing for homogeneous charging throughout the film. The potential drops between QD film and the reference electrode, in the electrolyte solution, resulting in a Fermi level in the QD film that is constant and equal to the Fermi level in the ITO electrode.

We use the convention that a decreasing voltage corresponds to a shift of the Fermi level toward vacuum. For all applied potentials reported in the main text, care was taken that the absorption of the unexcited sample did not change with respect to open circuit potential. This ensures that no charges were injected into quantum-confined levels, as they would lead to a bleach of the $1S_{3/2}1S_e$ absorption.[22,51,23]

■ ASSOCIATED CONTENT

Supporting Information

Dispersion correction of transient absorption data. Spectro-electrochemical determination of the absolute energetic position of the $1S_{3/2}$ level. Hole trapping rate constants and average electron rate constants. Derivation of capture and trapping rates. DFT calculations on the effect of ligand density. This material is available free of charge via the Internet at http://pubs.acs.org.

■ AUTHOR INFORMATION

Corresponding Author

*E-mail: A.J.Houtepen@tudelft.nl.

Author Contributions

S.C.B. and A.J.H. conceived the experiments and wrote the paper. J.M.A. and I.I. performed DFT calculations and aided in the interpretation of the results. Y.A. and F.C.G. facilitated the streak camera measurements. D.V. and L.D.A.S. aided in the interpretations of the results. All authors reviewed the manuscript.

Notes

The authors declare no competing financial interest.

■ ACKNOWLEDGMENTS

We thank W.H. Evers, M. Vermeulen, J. Thieme, and S. March for valuable assistance in realizing our experimental setups and L.T. Kunneman for supplying software used in the analysis of TA and PL data. We thank N. Renaud for inspiring discussions concerning the trapping mechanism. This work is part of the Joint Solar Programme (JSP) of HyET Solar and the Stichting voor Fundamenteel Onderzoek der Materie (FOM), which is part of The Netherlands Organisation for Scientific Research (NWO).

■ REFERENCES

(1) Panthani, M. G.; Kurley, J. M.; Crisp, R. W.; Dietz, T. C.; Ezzyat, T.; Luther, J. M.; Talapin, D. V. *Nano Lett.* **2013**, *14*, 670−675.
(2) Major, J. D.; Treharne, R. E.; Phillips, L. J.; Durose, K. *Nature* **2014**, *511*, 334−337.
(3) Donega, C. d. M. *Chem. Soc. Rev.* **2011**, *40*, 1512−1546.
(4) Califano, M.; Gomez-Campos, F. M. *Nano Lett.* **2013**, *13*, 2047−2052.
(5) Voznyy, O.; Thon, S. M.; Ip, A. H.; Sargent, E. H. *J. Phys. Chem. Lett.* **2013**, *4*, 987−992.
(6) Voznyy, O. *J. Phys. Chem. C* **2011**, *115*, 15927−15932.
(7) Voznyy, O.; Sargent, E. H. *Phys. Rev. Lett.* **2014**, *112*, 157401.
(8) Bozyigit, D.; Volk, S.; Yarema, O.; Wood, V. *Nano Lett.* **2013**, *13*, 5284−5288.
(9) Bozyigit, D.; Wood, V. *J. Mater. Chem. C* **2014**, *2*, 3172−3184.
(10) Katsiev, K.; Ip, A. H.; Fischer, A.; Tanabe, I.; Zhang, X.; Kirmani, A. R.; Voznyy, O.; Rollny, L. R.; Chou, K. W.; Thon, S. M.; Carey, G. H.; Cui, X.; Amassian, A.; Dowben, P.; Sargent, E. H.; Bakr, O. M. *Adv. Mater.* **2014**, *26*, 937−942.

DOI: 10.1021/acs.nanolett.5b00050
Nano Lett. 2015, 15, 3056−3066

(11) Voznyy, O.; Zhitomirsky, D.; Stadler, P.; Ning, Z.; Hoogland, S.; Sargent, E. H. *ACS Nano* **2012**, *6*, 8448−8455.
(12) Rinehart, J. D.; Weaver, A. L.; Gamelin, D. R. *J. Am. Chem. Soc.* **2012**, *134*, 16175−16177.
(13) Weaver, A. L.; Gamelin, D. R. *J. Am. Chem. Soc.* **2012**, *134*, 6819−6825.
(14) Brovelli, S.; Galland, C.; Viswanatha, R.; Klimov, V. I. *Nano Lett.* **2012**, *12*, 4372−4379.
(15) Brovelli, S.; Bae, W. K.; Meinardi, F.; Santiago González, B.; Lorenzon, M.; Galland, C.; Klimov, V. I. *Nano Lett.* **2014**, 486−494.
(16) Galland, C.; Ghosh, Y.; Steinbruck, A.; Sykora, M.; Hollingsworth, J. A.; Klimov, V. I.; Htoon, H. *Nature* **2011**, *479*, 203−207.
(17) Galland, C.; Ghosh, Y.; Steinbrueck, A.; Hollingsworth, J. A.; Htoon, H.; Klimov, V. I. *Nat. Commun.* **2012**, *3*, 908.
(18) Qin, W.; Liu, H.; Guyot-Sionnest, P. *ACS Nano* **2014**, *8*, 283−291.
(19) Qin, W.; Shah, R. A.; Guyot-Sionnest, P. *ACS Nano* **2012**, *6*, 912−918.
(20) Qin, W.; Guyot-Sionnest, P. *ACS Nano* **2012**, *6*, 9125−9132.
(21) Boehme, S. C.; Walvis, T. A.; Infante, I.; Grozema, F. C.; Vanmaekelbergh, D.; Siebbeles, L. D. A.; Houtepen, A. J. *ACS Nano* **2014**, *8*, 7067−7077.
(22) Vanmaekelbergh, D.; Houtepen, A. J.; Kelly, J. J. *Electrochim. Acta* **2007**, *53*, 1140−1149.
(23) Boehme, S. C.; Wang, H.; Siebbeles, L. D. A.; Vanmaekelbergh, D.; Houtepen, A. J. *ACS Nano* **2013**, *7*, 2500−2508.
(24) Efros, A. L.; Rodina, A. V. *Phys. Rev. B* **1993**, *47*, 10005−10007.
(25) Klimov, V. I. *J. Phys. Chem. B* **2000**, *104*, 6112−6123.
(26) Kambhampati, P. *J. Phys. Chem. C* **2011**, *115*, 22089−22109.
(27) Saari, J. I.; Dias, E. A.; Reifsnyder, D.; Krause, M. M.; Walsh, B. R.; Murray, C. B.; Kambhampati, P. *J. Phys. Chem. B* **2012**, *117*, 4412−4421.
(28) Malko, A. V.; Mikhailovsky, A. A.; Petruska, M. A.; Hollingsworth, J. A.; Klimov, V. I. *J. Phys. Chem. B* **2004**, *108*, 5250−5255.
(29) McArthur, E. A.; Morris-Cohen, A. J.; Knowles, K. E.; Weiss, E. A. *J. Phys. Chem. B* **2010**, *114*, 14514−14520.
(30) de Mello Donegá, C.; Koole, R. *J. Phys. Chem. C* **2009**, *113*, 6511−6520.
(31) Chen, S.; Wang, L.-W. *Chem. Mater.* **2012**, *24*, 3659−3666.
(32) Jasieniak, J.; Califano, M.; Watkins, S. E. *ACS Nano* **2011**, *5*, 5888−5902.
(33) Jones, M.; Lo, S. S.; Scholes, G. D. *Proc. Natl. Acad. Sci. U.S.A.* **2009**, *106*, 3011−3016.
(34) Jones, M.; Kumar, S.; Lo, S. S.; Scholes, G. D. *J. Phys. Chem. C* **2008**, *112*, 5423−5431.
(35) Talgorn, E.; de Vries, M. A.; Siebbeles, L. D. A.; Houtepen, A. J. *ACS Nano* **2011**, *5*, 3552−3558.
(36) Anderson, N. C.; Hendricks, M. P.; Choi, J. J.; Owen, J. S. *J. Am. Chem. Soc.* **2013**, *135*, 18536−18548.
(37) Anderson, N. C.; Owen, J. S. *Chem. Mater.* **2012**, *25*, 69−76.
(38) Morris-Cohen, A. J.; Malicki, M.; Peterson, M. D.; Slavin, J. W. J.; Weiss, E. A. *Chem. Mater.* **2012**, *25*, 1155−1165.
(39) Morris-Cohen, A. J.; Donakowski, M. D.; Knowles, K. E.; Weiss, E. A. *J. Phys. Chem. C* **2009**, *114*, 897−906.
(40) Knowles, K. E.; Tice, D. B.; McArthur, E. A.; Solomon, G. C.; Weiss, E. A. *J. Am. Chem. Soc.* **2009**, *132*, 1041−1050.
(41) Cohn, A. W.; Schimpf, A. M.; Gunthardt, C. E.; Gamelin, D. R. *Nano Lett.* **2013**, *13*, 1810−1815.
(42) Mooney, J.; Krause, M. M.; Saari, J. I.; Kambhampati, P. *Phys. Rev. B* **2013**, *87*, 081201.
(43) Bozyigit, D.; Jakob, M.; Yarema, O.; Wood, V. *ACS Appl. Mater. Interfaces* **2013**, *5*, 2915−2919.
(44) Knowles, K. E.; McArthur, E. A.; Weiss, E. A. *ACS Nano* **2011**, *5*, 2026−2035.
(45) Krause, M. M.; Mooney, J.; Kambhampati, P. *ACS Nano* **2013**, *7*, 5922−5929.
(46) Mooney, J.; Krause, M. M.; Saari, J. I.; Kambhampati, P. *J. Chem. Phys.* **2013**, *138*, 204705−9.
(47) Kloper, V.; Osovsky, R.; Kolny-Olesiak, J.; Sashchiuk, A.; Lifshitz, E. *J. Phys. Chem. C* **2007**, *111*, 10336−10341.
(48) Lebedev, M. V.; Misochko, O. V.; Dekorsy, T.; Georgiev, N. *J. Exp. Theor. Phys.* **2005**, *100*, 272−282.
(49) Dietzek, B.; Pascher, T.; Sundström, V.; Yartsev, A. *Laser Phys. Lett.* **2007**, *4*, 38−43.
(50) Ruch, P. W.; Cericola, D.; Hahn, M.; Kötz, R.; Wokaun, A. *J. Electroanal. Chem.* **2009**, *636*, 128−131.
(51) Houtepen, A. J.; Vanmaekelbergh, D. *J. Phys. Chem. B* **2005**, *109*, 19634−19642.

DOI: 10.1021/acs.nanolett.5b00050
Nano Lett. 2015, 15, 3056−3066